IN SEARCH OF THE PHYSICS: THE INTERPLAY OF EXPERIMENT AND COMPUTATION IN AIRFRAME NOISE RESEARCH; FLAP-EDGE NOISE

C.L. Streett, D.P. Lockard, B.A. Singer, M.R. Khorrami, and M.M. Choudhari
NASA Langley Research Center
Hampton, VA, USA

Abstract

The LaRC investigative process for airframe noise has proven to be a useful guide for elucidation of the physics of flow-induced noise generation over the last five years. This process, relying on a close interplay between experiment and computation, is described and demonstrated here on the archetypal problem of flap-edge noise. Some detailed results from both experiment and computation are shown to illustrate the process, and a description of the multi-source physics seen in this problem is conjectured.

Introduction

The importance of reducing subsonic approach airframe noise has now become apparent to the international community.[1] Civil air traffic continues to increase as does pressure from the public to control the resulting increase in landing noise, which is particularly annoying to those living in close proximity to airports. It is clear that noise reduction technology is critical to the future development and operation of the world's air transportation system.

Sound from an aircraft induced purely by airflow not related to the engine is known as airframe noise. During approach, its levels rival that of the engine, causing a threat to the successful certification of future subsonic aircraft. Over a broad range of flyover angles, particularly when the aircraft is directly overhead, virtually all of the noise heard is airframe induced.

NASA's Noise Reduction Program began an effort to study airframe noise (AFN) in 1995, in partnership with United States major airframe industries and academia. NASA Langley's role is to determine fundamental noise source mechanisms by relating sound generation to fundamental fluid mechanics. It is important to realize that airframe noise prediction methods employed in the past by industrial designers are based partly on broad-brush scaling estimates and partly on empirical data; little if any direct information regarding the actual noise generation mechanism is used, and for the most part, the details of these generation mechanisms remain unknown.

The task of elucidating the correct physics of a flow-induced noise mechanism is arduous, particularly in complex flowfields such as those around an aircraft high-lift system. To this end, the NASA Langley Airframe Noise team developed a multi-stage investigative process, which relies on continuous interplay between experiment and computation[2]. First, the steady flowfield must be understood, through a combination of detailed experiment and careful application of steady configuration RANS computations. The experimental aspect of this stage rests heavily on the use of microphone array technology[3] to localize regions of intense noise production. The corresponding configuration RANS computations must be of sufficient resolution to discern local flowfield features, but need not be so highly resolved that expense and time are overwhelming issues. Next, the flowfield is examined for features that are capable of producing large-amplitude organized fluctuations of the proper scale and frequency. In particular, flowfield features such as shear layers, jets, and vortices are known to potentially support inviscid inflectional instabilities, even in nominally turbulent flow. Such instabilities are powerful mechanisms for essentially converting steady vorticity concentrations into unsteady convecting disturbances of frequencies commensurate with the scale of the steady flowfield structure that engendered them. The nonlinear interaction of these fluctuations, and/or the evolution of these fluctuations in a rapidly varying mean flow, are mechanisms for noise generation by these fluctuations.

The next stage of the LaRC AFN investigative process is the development of simplified models, ones for which the basic underlying physical mechanisms of noise generation in the complex flowfield under study are highlighted in a simpler setting than the original configuration flowfield. For instance, in the case of flap-edge noise, the problem that serves as the example in this paper, tests conducted at Boeing and the then-McDonnell Douglas of subsonic transport configurations with high-lift systems deployed showed that the flap-edge region produced significant airframe noise. Tests conducted first at NASA ARC[4] and subsequently at LaRC using an unswept wing with a

simple part-span flap showed similar (but not identical) noise production characteristics; such simplified geometries permitted the computational study that is discussed here. The computational studies expanded the understanding of the underlying noise generation mechanisms, and showed where Reynolds number- and configuration-dependent differences between full configuration and simple model testing were to be expected, and why. The simplified-model testing is invaluable, however, in that the essential physics can be elucidated and studied in detail both experimentally and computationally, permitting better understanding of the physical processes that would be required for physics-based predictive modeling. In addition, understanding of these physical processes can identify mechanisms that could be exploited or interrupted for noise reduction. Often, a conjecture is made on the specific noise source physics based on this understanding, and a noise-reduction modification is conceived that aims selectively at that mechanism. Further testing with that modification in place then gives strong evidence as to the correctness of the original conjecture. Such testing, along with comparisons of noise feature details such as source location, spectral shape, and directivity, is the final stage of the LaRC-developed investigative process.

In the remainder of this paper, we will focus on the archetypal problem of flap-edge noise; we shall describe some concepts regarding numerical simulation of noise generation mechanisms, and demonstrate these concepts for the flap-edge noise problem. We will then show how experimental results can focus these simulations on the relevant noise source areas, how the development of simplified configurations is directed by steady RANS computations, and how the interplay between unsteady numerical simulations and detailed experiments on these simplified models can lead to understanding of the physics of the noise sources that are present for the original configuration.

Prediction of Flow-Induced Noise

Although the subject of considerable study for the case of jet flows[5], the direct prediction of the noise produced by locally separated flows on aircraft components through the use of numerical simulation had received comparatively little attention before 1998. Additionally, such flowfields tend to be rather complex in their mean, thus experimental investigations of the fluctuations occurring in these flows are also lacking. Both of these shortfalls result from the spatial and temporal resolution that would be required for a complete description of the mean and fluctuating flowfield. For example in Ref. 6, steady Reynolds-averaged Navier-Stokes (RANS) calculations are

compared with experimental results for a simple part-span flap model of a high-lift system. The computation, using the well-established code CFL3D[7], required a mesh of over 19 million grid points for adequate spatial resolution of the flowfield; these results are used in this study as a mean state for the computation of an approximate fluctuating flowfield, as will be described. Although this large computation (for its time), requiring about 50 hours of Cray C-90 CPU time, provides good spatial resolution of the steady flowfield, it is completely inadequate to accurately capture the majority of the fluctuations that are believed to generate noise in this flow. Additionally, these fluctuations are known to be broadband in frequency. Since the computational effort required to simulate unsteady phenomena is roughly proportional to the ratio of the highest-to-lowest frequencies, it is clear that the use of unsteady RANS to simulate these fluctuations is even presently quite expensive. In addition, the use of unsteady RANS must face issues such as the calibration of the turbulence model for capturing unsteady flows. Some promising results, however, are presented in a companion paper[8], and in Ref. 9.

Thus, it is clear that in order to provide some detailed estimate of the origin and frequency content of fluctuations in a complex aerodynamic flowfield such as that occurring about the high-lift system of a commercial subsonic transport aircraft, let alone directly predicting the noise generated by such a flowfield, some approximation is required. For the computation of flap-edge noise described in this study, three major approximations were used to reduce the problem to a level that allows at least a rough estimate of the frequency content and directivity of the noise generated by the flow at the side edge of the flap of a high-lift system. Although approximate, these estimates are based on simulations of the true physical phenomena that generate the noise, and are of reasonable computational cost that parameter studies are possible.

This first approximation comes in the invocation of the Lighthill acoustic analogy[10]. As will be seen in the following section, this allows the combined noise generation and propagation problem, as would be solved in a so-called "direct computational aero-acoustics" simulation using the unsteady compressible Navier-Stokes equations[8,9], to be divided into a computation of the fluctuations in the near field and a separate computation of the generation and propagation of the noise. The former computation is still somewhat too large to be manageable, due to the resolution requirements discussed above, requiring further approximation. The second approximation lies in the use of the incompressible Navier-Stokes equations to simulate the near-field fluctuations. As the

local Mach numbers seen in the flap-edge flowfield are generally below 0.3 for typical applications, this is considered reasonable. However, with the use of an incompressible method for computing the hydrodynamic fluctuations in the flowfield, the computation of the sound generated by these fluctuations must be carried out using information from the entire field, rather than just on the solid surfaces[11]. The reduction in computational effort afforded by the incompressible flow approximation is still less than required to allow for a full simulation of the near-field fluctuations in this complex flow. In this study, therefore, the use of a "temporal" approximation is used to reduce the simulation of the full three-dimensional flowfield into a series of two-dimensional simulations; this approximation will be discussed and justified in later sections.

Lighthill's Acoustic Analogy

What follows is a very brief and incomplete description of the fundamentals of Lighthill's acoustic analogy, in order to illustrate how the theory allows, at least conceptually, for the noise source and propagation mechanisms to be separated. The reader is referred to the original reference[10] and works by Ffowcs-Williams[11] for more complete descriptions.

The basis of the theory is an exact expression of the compressible Navier-Stokes equations. In the absence of boundaries and mean flow, this equation is:

$$\frac{\partial^2 \rho'}{\partial t^2} - c_o^2 \frac{\partial^2 \rho'}{\partial x_i^2} \;=\; \frac{\partial^2}{\partial x_i \partial x_j}\left(\rho_o u_i u_j\right)$$

The LHS of the equation is clearly a linear wave equation, and depicts the propagation of density fluctuations due to sound. The RHS, which results from the nonlinear convection terms in the momentum equation, acts as a source to the medium outside the region of fluctuating flow. This source is assumed known, derived from solutions or estimates of the nearfield fluctuating flow.

In the presence of (stationary) boundaries, an additional, surface source term appears [5]:

$$\frac{\partial}{\partial x_i}\left[p_{ij}\, \delta(f)\, \frac{\partial f}{\partial x_j} \right]$$

where $f=0$ defines the surface, and p_{ij} contains the (compressible) fluctuating surface pressure and viscous stresses. If the surface pressure available carries no acoustic information, such as would be the case when the nearfield fluctuations are computed using an incompressible framework, then this term should not be included, and the volume term only used as the source. However, the solution of the Lighthill wave equation must include the effects of the solid boundaries, particularly when sharp corners are present.

Flap-Edge Flowfield

Based on both experimental and computational studies, a fair understanding of the steady flowfield in the vicinity of the edge of a flap of a high-lift system has been gained. Clearly, the difference in lift between flapped and unflapped sections of a wing with a part-span flap will result in a trailing vortex emanating from near the flap edge, as shown in Fig 1 which depict the streamlines wrapping around the flap side edge.
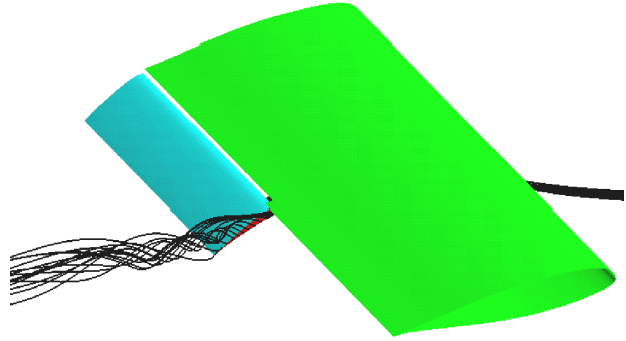

Figure 1. Streamlines in flap-edge flowfield

The details of the development of this vortex are surprisingly complex. Shown in Fig. 2 are contours of a quantity that approximates the streamwise component of vorticity, displayed in planes normal to the flap edge and chord line, denoted "crossflow" planes. As can be seen, the pressure difference between the upper and lower surfaces of the flap creates flow around the edge. Two separation bubbles, with associated streamwise vorticity and rollup, are created at the upper and lower corners of the flap edge. The reattachment point of the side-edge vortex moves up the edge as the flow progresses down the flap, eventually reaching the upper corner. The side-edge vortex then travels over the upper corner, interacting and eventually merging with the upper-surface vortex. This leaves a single trailing vortex, which is continually fed with vorticity from the cylindrical shear layer that emanates from the lower edge corner. This mechanism of continual feed of vorticity into the vortex produces a strong jet-like flow in the core of the vortex, where streamwise velocities of over twice the freestream velocity have been measured.

The flowfield vorticity shown in Fig. 2 were derived from 5-hole probe measurements[12]. Corresponding RANS results[6] are shown in Fig. 3, using the same scale on vorticity. Note that while the vortex-core strength is not predicted well in the most chordwise distant cut (due to turbulence modeling issues, we believe), the evolution and strength of the vortices near the flap side edge compare very well.
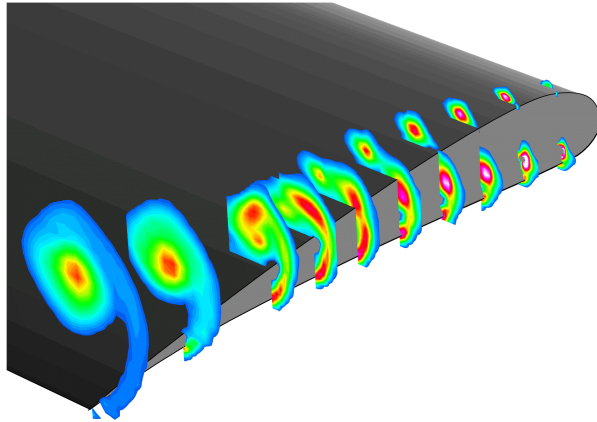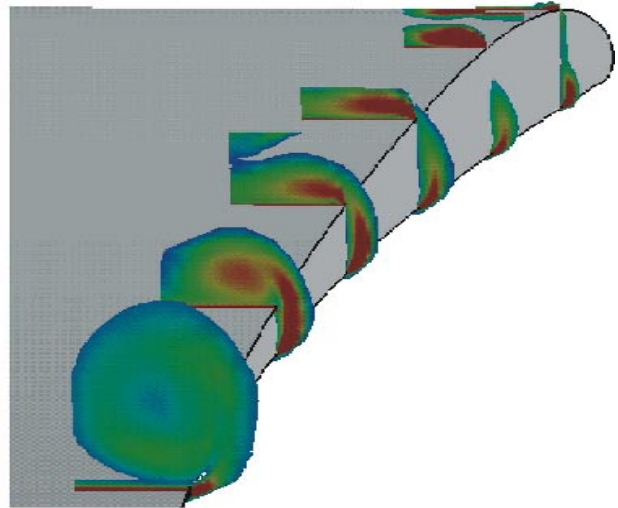

Figure 2. Streamwise vorticity near the flap edge, from 5-hole probe measurements.
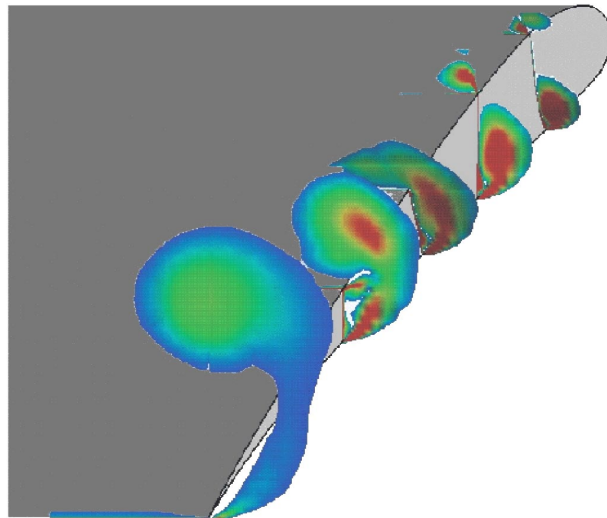
Figure 3. Streamwise vorticity near the flap edge, from steady RANS computations.

For this flap section, which was chosen for a building-block study due to its simple geometry, the trailing vortex leaves the flap surface and is more than a vortex-diameter clear of the surface when it reaches the trailing-edge location. For other, more representative flap sections such as that used in a high-Reynolds number experiment in the LTPT[13], careful RANS computations indicate that the vortex may remain in the vicinity of the surface or upper corner until reaching the trailing edge, as illustrated in Fig. 4, which should be compared with Fig. 3. This has implications in the amount of noise generated by fluctuations that develop in the vortex/shear-layer system, as will be discussed later.

Figure 4. Streamwise vorticity near the flap edge, from steady RANS computations; LTPT configuration.

Another computation/experiment comparison may be made in terms of the surface pressure near the flap edge. Shown in Fig. 5 is the comparison between measurements using pressure sensitive paint and the corresponding computed results, again using the same scale. Good agreement is seen, both in terms of the shape of the surface-pressure "footprint" of the vortex, and its magnitude.

A final, and most difficult test of the capability of the RANS computations to reproduce this complex flowfield, and thus permit further analysis of the development of fluctuations leading to noise, is the comparison against a plane of mean velocities measured using particle image velocimetry. This comparison is a rigorous test since not only must the flowfield features and their magnitudes must be predicted correctly, but also the position of the vortex must be correct. Even if the vortex is displaced only very slightly, a lack of agreement will be seen. It is known that vortex position is highly sensitive to small perturbations, and this comparison attests not only to the veracity of the computations, but also to the care with which the 5-hole probe measurements of Ref. 12 were made.
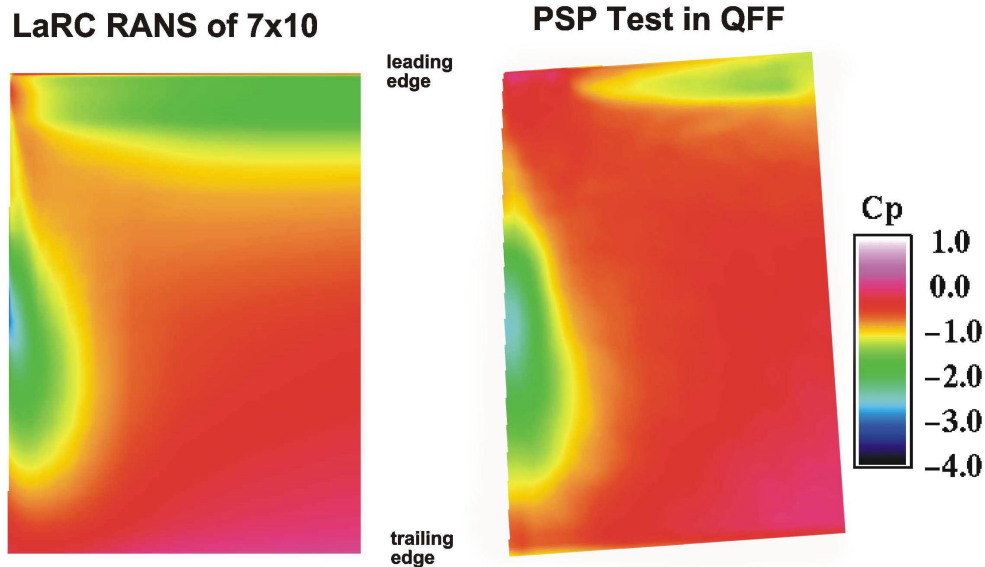
American Institute of Aeronautics and Astronautics

LaRC RANS of 7x10

PSP Test in QFF

leading
edge

Cp
1.0
0.0
-1.0
-2.0
-3.0
-4.0

trailing
edge

Figure 5. Comparison of surface pressures from RANS computation and from PSP measurements.

Streamwise Velocity
$d_f = 39°$
Plane at flap edge

RANS

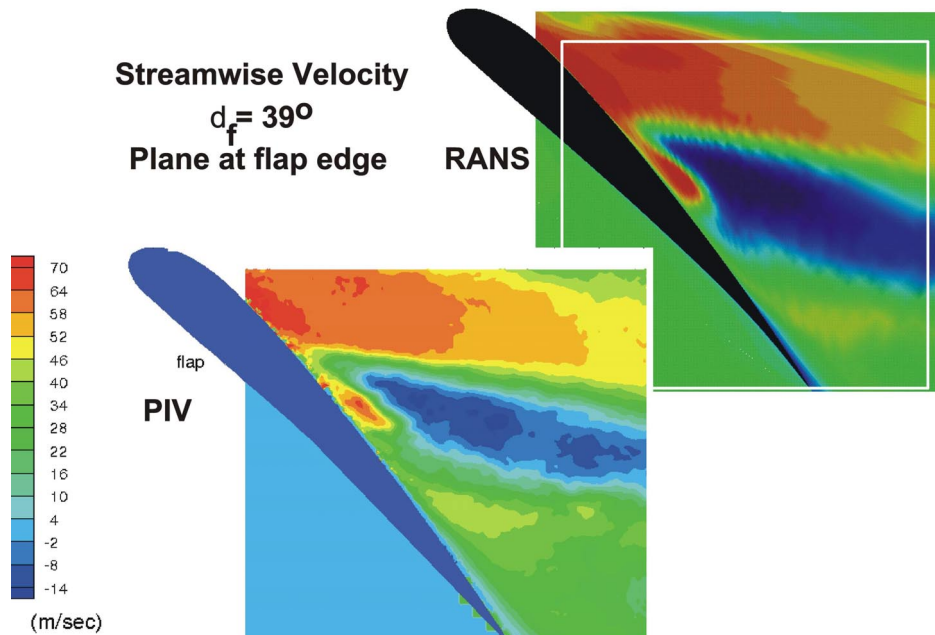70
64
58
52
46
40
34
28
22
16
10
4
-2
-8
-14

(m/sec)

flap

PIV

Figure 6. Comparison of streamwise velocity in plane at flap edge, from PIV measurements and from RANS.

Numerical Simulation Algorithm

It was necessary to reduce the size of the numerical simulation in order to be able to conduct as many as were required to give guidance as to the sensitivity of the development of hydrodynamic fluctuations in this complex flowfield. Assuming that it is possible to justify performing simulations in the crossflow plane only (as will be discussed in the following section), we decided to compute unsteady incompressible Navier-Stokes solutions in a geometry that includes the rectilinear end of the flap. A robust and highly accurate algorithm for such solutions is described in Ref. 14; the physical domain is divided into rectangular sub-domains as required, and tensor-product Chebyshev spectral collocation of the pertinent equations is employed in each sub-domain. Each simulation required about 4 hours of SGI (1998 vintage) workstation time to reach statistical steady state. Details are given in Ref. 14.

Temporal Simulation Technique

Consider a fluctuating disturbance with streamwise scale $O(\varepsilon)$, evolving in a mean flowfield

American Institute of Aeronautics and Astronautics

which changes in the streamwise direction on a $O(1)$ length scale. This disturbance additionally has an $O(1/\varepsilon)$ frequency, and convects at some $O(1)$ fraction of the mean velocity. For this situation, it is clear that a multiple-scales analysis is justified; the disturbance undergoes $O(1)$ changes in the time and distance for which the mean state changes by only $O(\varepsilon)$. This formalism has been extensively employed in the area of simulations of transition to turbulence in boundary layers.

Another way to look at the temporal simulation framework is to consider a computational frame that travels downstream at a constant speed. In this frame, the mean state appears to change on a long, $O(1)$ time scale, whereas the disturbance, due to its $O(1/\varepsilon)$ frequency, evolves on an $O(\varepsilon)$ time scale. In this case, the mean state may be considered as frozen. The implication in regard to the physics of the disturbance is that gradients that matter to the development of the disturbance lay only in the transverse, and not streamwise, direction.

From this we conclude that, to some level of approximation, the evolution of the disturbances resulting from the fundamental instability of the vortex / cylindrical shear layer system may be considered within a frozen mean state. This is a significant step toward the analysis of flowfields that are truly representative of those near the edge of flaps in high-lift systems; we may extract crossflow "cuts" from high-resolution steady RANS computations, and perform simulations using these solutions as the mean flowfield within which the disturbances that are conjectured to create noise will evolve. Results from such analysis are shown in the following section.

Computational Results

Cylindrical Shear Layer Instability

We utilize the RANS solutions described above as mean flowfields for disturbance simulations, interpolating the RANS solutions onto the spectral multi-domain discretization topology described earlier. These interpolations are carried out in planes that are taken to be roughly normal to the axis of the vortex system. These simulations were intended to provide an indication of the strength of the instability mechanism at work in this flowfield; what matters is the amount of amplification that the inflectionally unstable flowfield provides, as a function of frequency. The flowfield details that influence this instability, the strength, location, and thickness of the cylindrical shear layer, for instance, are functions of the configuration and loading. Details are given in Ref. 14.

In a plane at approximately 50% flap chord, the side-edge and top vortices have merged, and the cylindrical shear layer / vortex system is well established. Contours of mean and disturbance vorticity are shown in Fig. 7, again with three model frequencies of 5, 15, and 30 kHz forcing. The instability of the cylindrical shear layer is quite apparent, with the 5 kHz disturbances persisting with significant magnitude even as they are convected over the vortex. Maximum disturbance vorticity magnitudes in the shear layer are roughly equal for the three frequencies, demonstrating the broadband nature of the instability. Note also how the shear-layer disturbances appear to have different characteristics whether they are of low or high frequency. At low frequencies, the disturbances appear to involve both the shear layer and the outer and upper parts of the vortex itself, whereas at higher frequencies the disturbances only grow in the initial part of the shear layer. Thus, we consider the shear-layer instabilities to be comprised of two distinct families of modes, implying that there would be a double-humped appearance to the noise spectrum created by these disturbances, and that noise reduction concepts would have to be tailored separately for the two families.
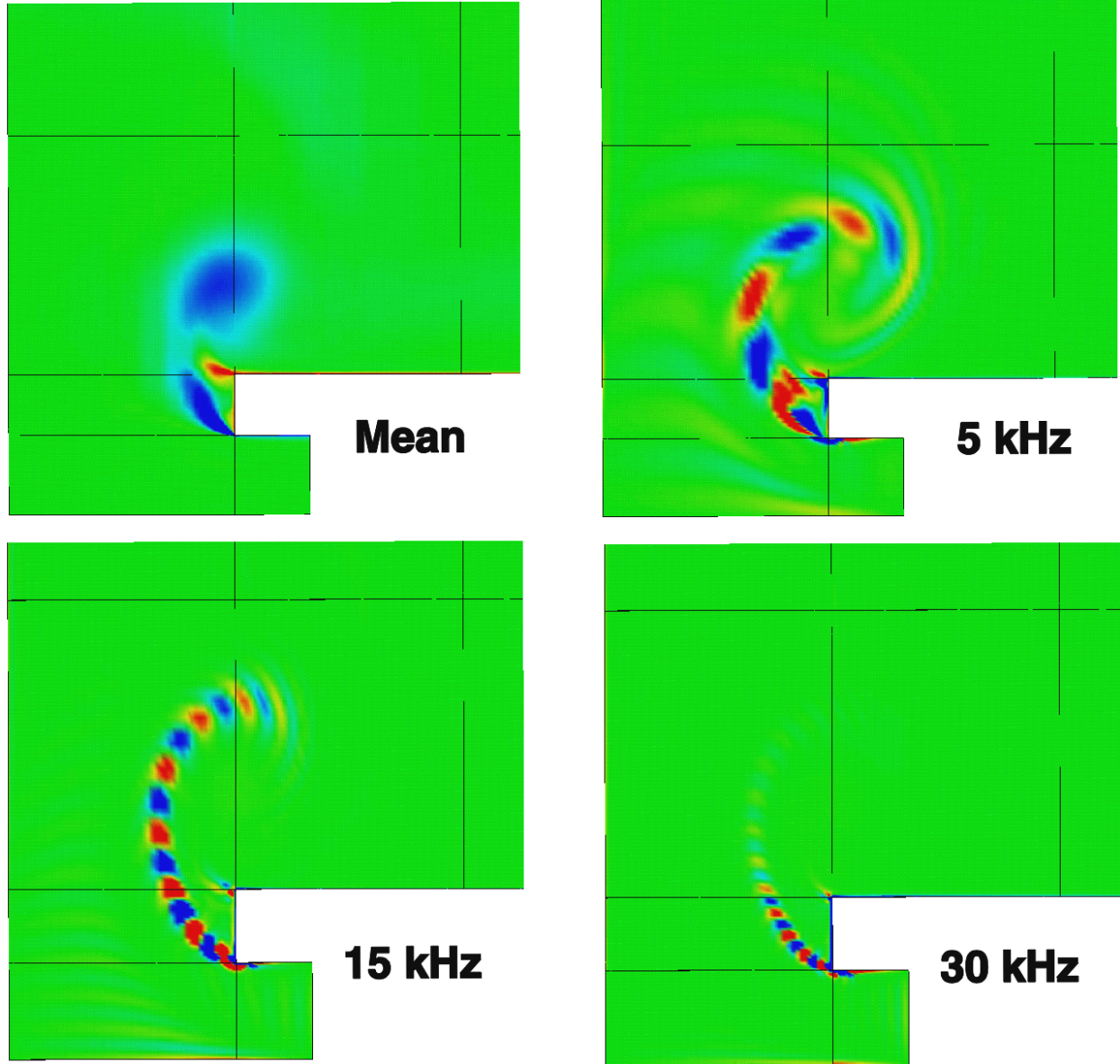
Figure 7. Contours of mean and disturbance vorticity, 50%-flap chord station.
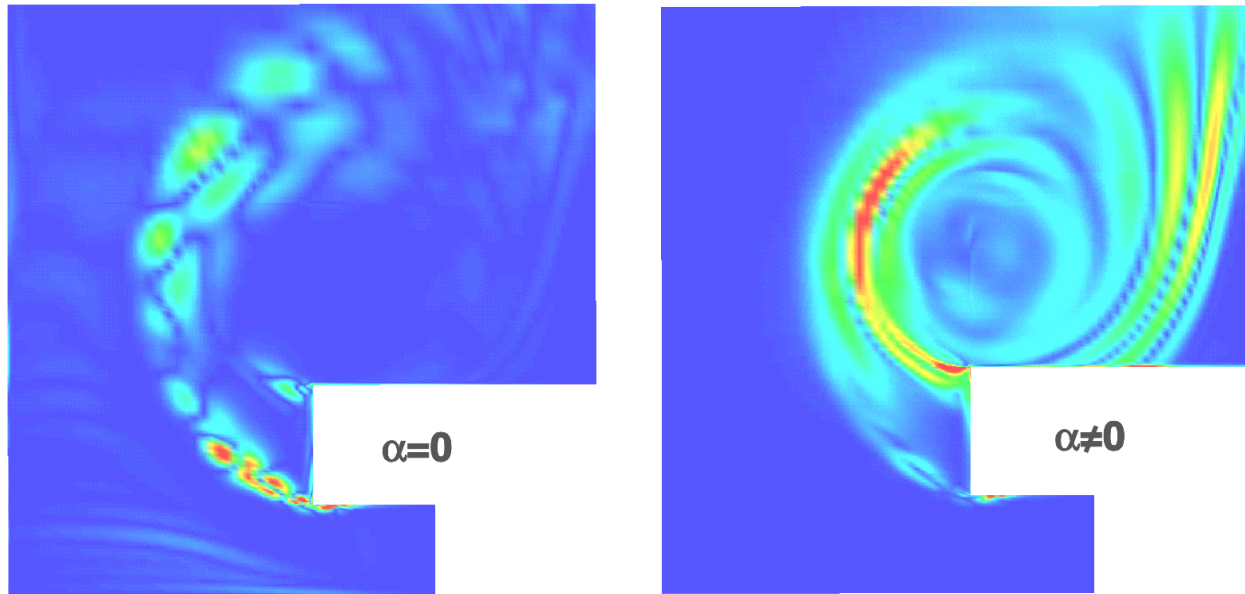
Vortex Instability

In the above simulations, it is assumed that the disturbances have no variation in the direction normal to the crossflow plane that is cut from the RANS solution. While this is a reasonable assumption for the instabilities that result from the cylindrical shear layer, it is conjectured that instabilities should exist also in the shear of the vortex itself, especially in light of the strong jet-like flow in the core of the vortex. Further, the disturbances resulting from this vortex instability should have significant oscillation in the streamwise direction. Assuming that the spatial scale of such oscillation is small compared with the scale of variation in the streamwise direction of the mean flow, then we

can apply the additional *ansatz* that these oscillations are homogeneous in that direction in the simulation. For the following simulations, therefore, we discretize the three-dimensional Navier-Stokes equations, and replace all $\partial/\partial x$ terms by $i\alpha$, where α is a prescribed streamwise wavenumber parameter. The full three-dimensional RANS solution, interpolated onto a crossflow plane as before, is taken as the mean state, and the (complex) equations are discretized in the crossflow plane and time advanced as before.

With this assumption, the parameter space to be explored now has two parameters: frequency and streamwise wavenumber, with the results shown earlier corresponding to the case $\alpha=0$. Although this study was

American Institute of Aeronautics and Astronautics

not exhaustive, it was found for the most part that the shear-layer instabilities are maximally amplified for $\alpha=0$. However, there exists a separate family of instabilities, associated with the conjectured vortex-instability mechanism; the streamwise wavenumber for these disturbances is fairly high, corresponding to wavelengths on the order of ¼ to ½ of the vortex diameter. The dominant frequency band of these disturbances is considerably lower than that for the shear-layer instability; in model frequencies, the shear-layer instability band was roughly 5 to 30 kHz, whereas the vortex instability band is about 1 to 10 kHz. In Fig. 8 is shown a comparison of snapshots of disturbance vorticity for the two disturbance modes, using broadband forcing for each simulation; the vortex mode has a streamwise wavelength of 1/3 of the vortex diameter. Note that the vortex disturbance has a ring-like structure. This is more clearly discernable in Fig. 9, in which isolevel surfaces of disturbance vorticity are shown for these same modes.

Figure 8. Disturbance vorticity snapshots; shear-layer and vortex instability modes.
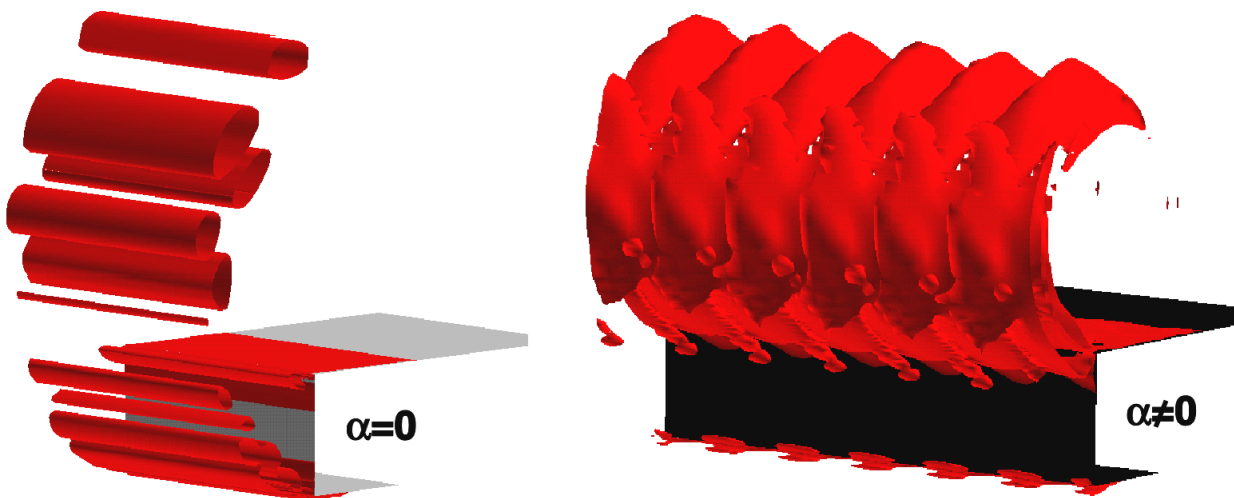
**Figure 9. Isolevel surfaces of disturbance vorticity; shear-layer and vortex instability modes.**

These vortex disturbance modes have implication in the generation of noise for flap configurations for which the vortex remains in proximity to the flap surface all of the way to the trailing edge; as noted above, realistic flap sections frequently show this behavior. As these disturbances

American Institute of Aeronautics and Astronautics

convect past the trailing edge, they would be expected to have considerable amplitude and be quite coherent in the spanwise direction; thus, it would be expected that a significant amount of locally enhanced trailing-edge noise would result. This expected streamwise coherence was confirmed experimentally; results from a sequence of surface pressure transducers near the flap side edge in a high-Reynolds number test[13] show strong coherence at a frequency that agrees with the computational results – 4kHz in this case. The noise produced by this disturbance mode will be discussed later.
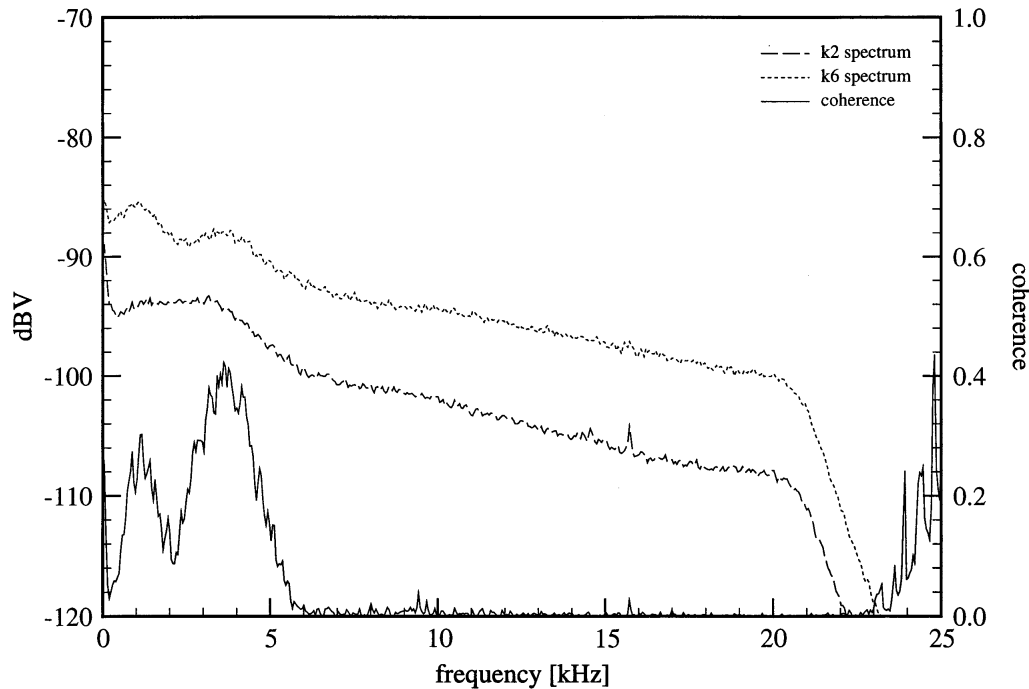
Figure 10. Spectra and coherence of two surface pressure measurements in line near flap side edge, showing evidence of vortex disturbance mode.

Noise Generation by Shear-Layer Instability

In an attempt to test whether the fluctuations predicted by the above method are related to the noise generated by a flap-edge flowfield, the RHS of Eq. 1 (the so-called Lighthill stress tensor) was computed for a number of single-frequency simulations at the 50% flap-chord station shown in Fig. 7. Contours of the Lighthill stress tensor are given in Fig. 11, from the 15kHz simulation shown in Fig. 7. Note that the strongest concentration of this quantity occurs near the corner where the cylindrical shear layer originates; this is due to the rapidly changing amplitude and spatial wavenumber of the disturbance in that region, resulting from the strong variation in shear-layer thickness in that region.
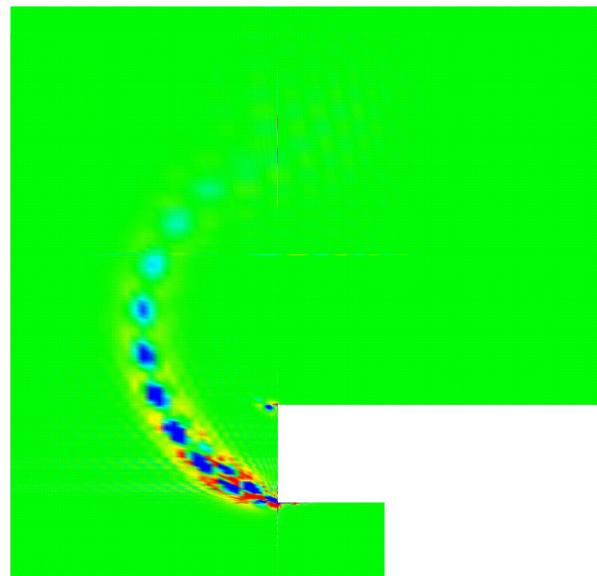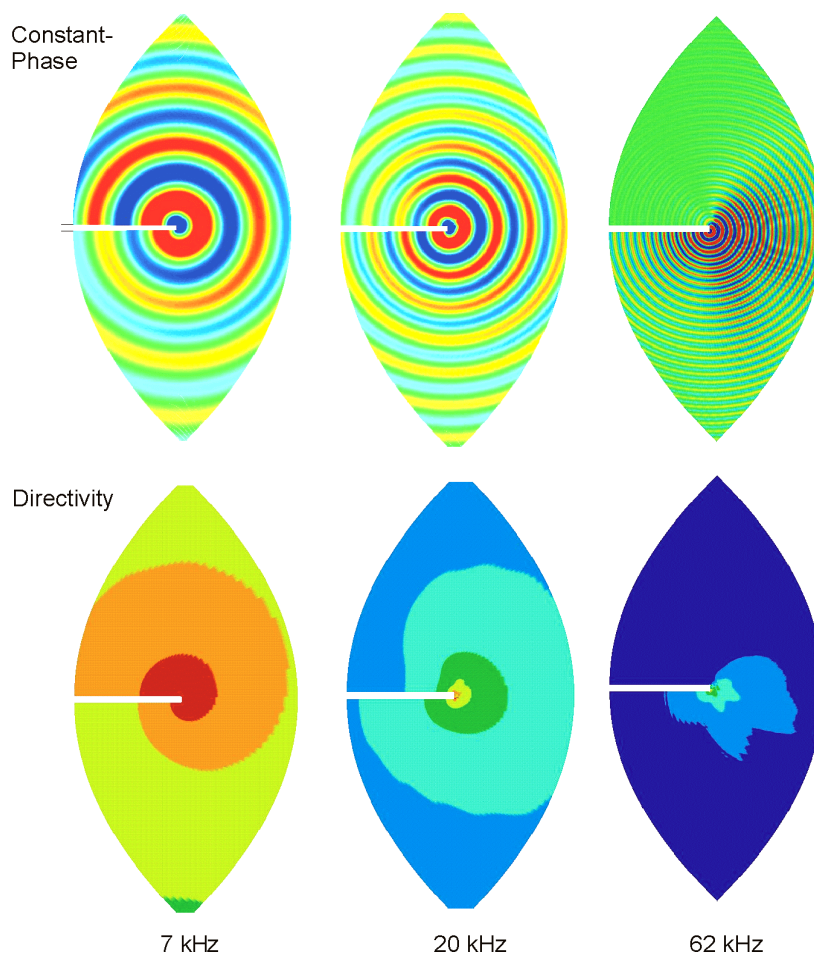

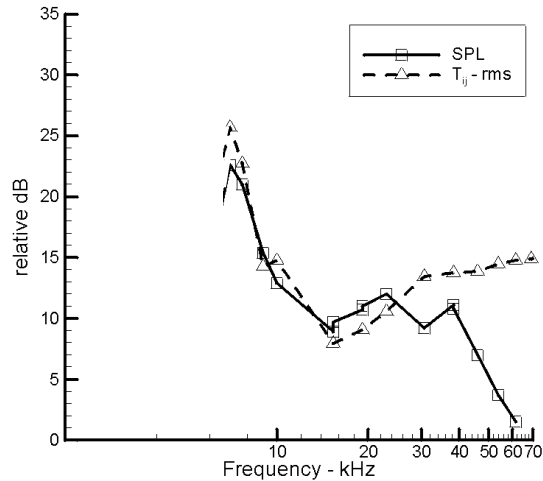**Figure 11. Contours of Lighthill stress tensor, 15kHz simulation.**

The resulting acoustic field was then computed using a high-order accurate harmonic wave equation solver, forced by the computed Lighthill stress tensor; the finite-thickness flap-edge geometry was approximated by way of a conformal mapping to the infinite half-plane. Results for three frequencies are shown in Fig. 12, in terms of constant-phase contours, which show the resulting acoustic wave pattern, and in terms of contours of $20 \log(\mathrm{mag}(\rho'))$, which gives an indication of directivity. Each contour level in the latter display is 5 dB. Note how the directivity pattern rotates with frequency, from stronger upward radiation for the lowest frequency, to a relatively flat pattern that favors the downward direction for the intermediate frequency, to a primarily downward pattern with several irregularities for the highest frequency.

One may choose a convenient location in the acoustic field at which to interrogate a sequence of simulations over a range of frequencies, and thus obtain a representative spectrum of the noise produced by the cylindrical shear-layer mechanism. Results for the point (0, -10), i.e., ten edge-thicknesses straight down from the edge, are labeled in Fig. 13 as "SPL". While results below 8 kHz are questionable, the spectrum shows the following features: a falloff from the maximum starting at about 10kHz, a flattening of the spectrum from about 14 to 35 kHz, and a rapid falloff beyond that point.. These results are compared with the quantity $20 \log(<T_{ij}>)$, which shows the former behaviors but not the falloff. This indicates that the higher-frequency fluctuations, while still strong, are not efficient generators of noise. This is potentially because these small wavelength disturbances are not strongly distorted on their own scale by the rapidly growing mean shear layer. Such rapid distortion is the only way in which linear disturbances with subsonic phase speed can scatter energy into modes that propagate at sonic speed. The apparently double-humped nature of the noise spectrum is indicative of the distinct natures of the low- and high-frequency shear-layer disturbance families.

Figure 12. Wave and directivity patterns from acoustic computation.

Figure 13. Comparison of amplitude of Lighthill stress tensor and radiated sound.

The above simulations gave considerable insight as to the source mechanisms involved in flap-edge noise. Per the LaRC investigative process, comparison of details between experimental and computational results using the simplified building-block geometry followed. Indeed, while the above simulations described in more detail in Ref. 14 showed good agreement with the experimental results of Ref. 15, data from the high Reynolds-number tests of Ref. 13 showed additional elements in the flap-edge noise spectrum. An example spectrum is shown in the center of Fig. 14. Note that in addition to the broadband component – presumably related to the shear-layer instability mechanism – there are the additional features of a low-frequency narrow spike, and a high-frequency broadband feature. Using equivalent source location maps from microphone acoustic array measurements[3,13], we can characterize these spectral features as to their apparent source locations; the maps shown in Fig. 14 are planform planes, with the unflapped main element trailing-edge region on the left, and the flap with main trailing edge on the right. The middle broadband spectral component is associated with source locations lateral to the flap-side edge and ahead of the trailing edge, as would be expected for shear-layer disturbance noise. The low-frequency spike appears to be located at or aft of the flap trailing edge, inboard but near the side edge. Since the vortex instability mode discussed above would appear as a locally enhanced trailing-edge noise source, the source location from these array data is consistent with the conjectured correspondence.

The final spectral feature seen in Fig. 14, the high-frequency broadband component, is localized by the array as being comprised of sources in the shear-layer instability region, but also in the region where the lateral edge of the unflapped main trailing edge is next to, but above, the leading edge of the flap – what we here call the "side-lap region". Aerodynamic analysis of the flowfield in this area shows that a spanwise shear layer is created in that region, driven by the pressure difference between the high pressure under the unflapped main trailing edge and the low pressure above the flap leading edge. A cross-sectional cut through this region of the CFD data in Fig. 15 shows the detail of this lateral shear layer, which feeds the weak trailing vortex engendered by the lift difference between the unflapped and flapped sections of the main element. The sign of this vortex is opposite that of the flap-edge vortex, and appears to be swallowed by the latter farther downstream. This spectral feature is quite Reynolds-number dependent; it appears only as the Reynolds number based on chord is increased to values within an order of magnitude of that of flight. Hence, this feature is not likely to be observed in low Reynolds number tests such as those in Refs. 4 and 15.

These spectral features have been found to be relatively universal across many configurations. Microphone array tests in 1997 of a commercial subsonic transport at high Reynolds number showed a flap-edge noise spectrum strikingly similar to that shown in Fig. 14, for example. Additionally, noise reduction modifications aimed at subtly interrupting each individual noise source mechanism have been developed, confirming that the final conjectures regarding the correspondence of spectral feature to source physics is correct. In many configurations, however, the low-frequency narrow spike is not observed. This can be explained by the flowfield differences illustrated in Figs. 3 and 4. When the flap-edge vortex breaks clear of the flap surface before the trailing edge, vortex instabilities cannot produce measurable noise due to their lack of a nearby scattering edge to convert hydrodynamic fluctuations into acoustic disturbances[16].

This understanding of the individual noise source mechanisms and their corresponding noise spectrum features finally led the LaRC AFN team to develop a notional model spectrum for flap-edge noise as shown in Fig. 16. In an actual flap-edge noise prediction method, the center frequencies and amplitudes of these four components must be estimated individually.

Thus, we have demonstrated the strength of considering both experimental and computational results together. The experimental results were used to locate the regions for a particular aircraft configuration where airframe noise is most strongly produced. Steady RANS computations indicated what flowfield features could be responsible for the noise generation, and

guided the design of a sequence of simplified configurations that embody the same relevant flowfield features as those of the full configuration. Detailed experimental measurements confirmed the presence of these flowfield features, and provided further information as to their noise characteristics, including frequency range and apparent source location. Approximate unsteady computations provided evidence that these flowfield structures did indeed support fluctuations of the measured frequency range, and that these hydrodynamic fluctuations were capable of producing noise. The final stage of such an investigation is to use the detailed knowledge of the physics of these individual sources to describe their sensitivities to wing-flap aerodynamic properties, to be used in a physics-based predictive model. This work is currently ongoing.
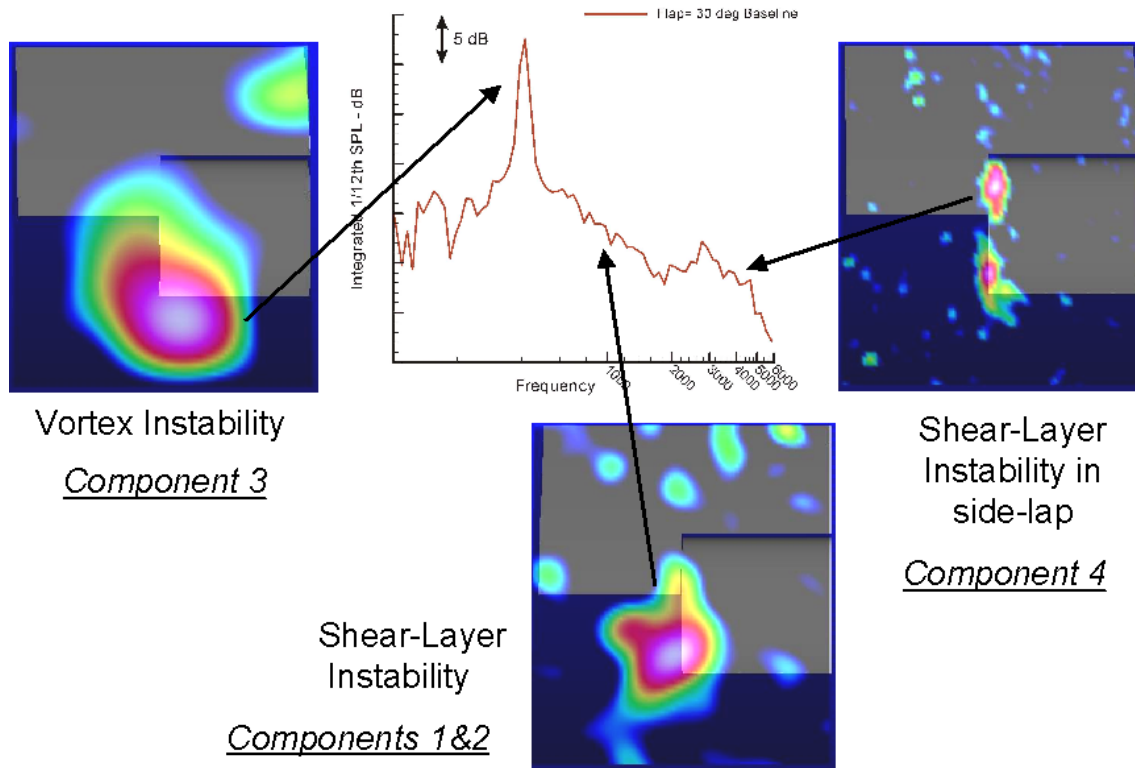

Figure 14. Flap-edge noise spectrum and equivalent source maps from array measurements; from LTPT experiment.
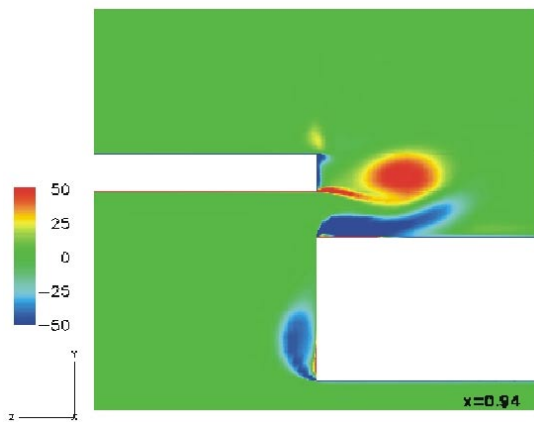

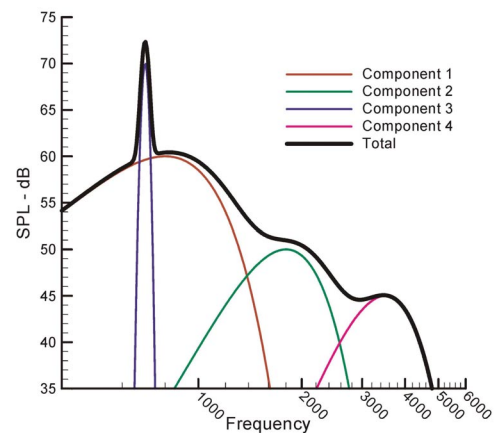**Figure 15. Cross-sectional cut of RANS solution, taken through "sidelap" region.**

Figure 16. Proposed model spectrum for flap-edge noise, based on source component physics.

Conclusions

The LaRC investigative process for airframe noise has been described, and demonstrated here on the archetypal problem of flap-edge noise. This process, relying on the close interplay between experiment and computation, consists of the following stages:

- Identification of strong noise source locations, using acoustic array measurements on a variety of aircraft configurations.
- Detailed investigation of steady flowfield in those source regions, to identify flowfield features that could support strong development of fluctuations. This requires both detailed experimental flowfield measurements and computations.
- Distillation of a simplified configuration, which highlights without complication these fluctuation-supporting flowfield features.
- Unsteady numerical simulations to confirm that fluctuations do indeed develop in such a flowfield and that they produce noise, and to characterize their sensitivities, spectral content, etc. These studies should be backed up by unsteady measurements, if possible.
- Confirm source physics conjectures by designing subtle flowfield modifications to interrupt the noise source mechanisms, without unduly disturbing the overall configuration aerodynamics.

As the process was stepped through in this paper, we showed the elucidation of the physics of multiple-component noise, demonstrating that neither experiment nor computation alone could have provided such insight on its own. In a companion paper[8], this process is demonstrated for the problem of the noise from a leading-edge slat.

Acknowledgement

References

1. Willshire, W.L. and Stephens, D.G.: "Aircraft Noise Technology for the 21st Century", NOISECON 98.
2. Macaraeg, M.M.: "Fundamental Investigations of Airframe Noise," AIAA Paper 98-2224, June 1998.
3. Mosher, M.: "Phased Arrays for Aeroacoustic Testing – Theoretical Development," AIAA Paper 96-1713, 1998.
4. Storms, B. L., Ross, J. C., Horne, W. C., Hayes, J. A., Dougherty, R. P.,Underbrink, J. R., Scharpf, D. F., Moriarty, P. J., "An Aeroacoustic Study of an Unswept Wing with a Three-Dimensional High-Lift System," NASA TM 112222, Feb. 1998.
5. Morris, P.J., Wang, Q., Long, L.N., and Lockard, D.P.: "Numerical Predictions of High-Speed Jet Noise," AIAA Paper 97-1598, May, 1997.
6. Khorrami, M.R., Singer, B.A., and Radeztsky, R.H., "Reynolds Averaged Navier-Stokes Computations of a Flap Side-Edge Flow Field," AIAA Paper 98-0768, Jan. 1998.
7. Rumsey, C., Biedron, R., and Thomas, J.: "CFL3D: Its History and Some Recent Applications," NASA TM-112861, May 1997.
8. Khorrami, M.R., Choudhari, M.M, Singer, B.A., Lockard, D.P., and Streett, C.L.: "In Search of the Physics: The Interplay of Experiment and Computation in Slat Aeroacoustics," AIAA Paper 2003-0980, Jan. 2003.
9. Li, F., Khorrami, M.R., and Malik, M.R.: "Unsteady Simulation of a Landing Gear Flow Field," AIAA Paper 2002-2411, Jun. 2002.
10. Lighthill, M.J., "On Sound Generated Aerodynamically; I. General Theory," Proceedings of the Royal Society of London, Series A, Vol. 211, pp. 54-587, 1952.
11. Ffowcs-Williams, J.E., and Hawkins, D.L., "Sound Generation by Turbulence and Surfaces in Arbitrary Motion," Philosophical Transactions of the Royal Society of London, Vol. 264, No. A 1151, pp. 321-342, May 1969.
12. Radeztsky, R.H., Singer, B.A., and Khorrami, M.R., "Detailed Measurements of a Flap Side-Edge Flow Field," AIAA Paper 98-0700, Jan. 1998.
13. Choudhari, M.M. *et al*: "Aeroacoustic Experiments in the Langley Low-Turbulence Pressure Tunnel," NASA TM-2002-211432, Feb. 2002
14. Streett, C.L.: "Numerical Simulation of Fluctuations Leading to Noise in a Flap-Edge Flowfield," AIAA Paper 98-0628, Jan. 1998. See also: Streett, C.L.: "Numerical Simulation of a Flap-Edge Flowfield," AIAA Paper 98-2226, Jun. 1998.
15. Meadows, K.R., Brooks, T.F., Humphreys, W.M., Hunter, W.H., and Gerhold, C.H., "Aeroacoustic Measurements of a Wing-Flap Configuration," AIAA Paper 97-1595, May 1997.
16. Howe, M.S.: "A Review of the Theory of Trailing Edge Noise," Journal of Sound and Vibration, vol. 61, pp. 437-465, 1997.